Approximate lateral boundary conditions for turbulent simulations

By J. Jiménez AND C. Vasco[1]

Several synthetic lateral boundary conditions are tested on a direct numerical simulation in which only half of a turbulent channel is computed, with the boundary conditions being imposed at the central plane. This is motivated by the problem of matching large-eddy simulations to wall models. When the boundary contains no turbulent structure, a thin layer is created which decorrelates it from the flow, and the mean and fluctuating velocities are poorly represented. Introducing more structure, obtained by modifying velocity planes copied from the interior of the flow, improves the fluctuations, but the mean velocity profiles are still poor. This is traced to spurious pressure fluctuations which induce artificial energy fluxes, and can be partially avoided by approximately taking into account continuity in the generation of the boundary conditions. This third boundary condition gives good results for the velocity fluctuations, but some pressure and the mean velocity errors persist.

It is argued that the problem is related to that of imposing boundary conditions along characteristics in a hyperbolic system, and possible avenues for improvement are suggested.

1. Introduction

One of the problems of large-eddy simulations of complex flows is the high resolution required in the proximity of walls. The Reynolds shear stresses that determine the mean velocities are carried by the non-universal large turbulent scales. Sub-grid stresses in LES should be provided by the sub-grid model, but most present models do not reproduce the shear stresses well (Jiménez & Moser 1998). The simulations should therefore be designed so that most of the shear stresses are carried by the resolved eddies, and this implies that the filters should not be wider than a fixed small fraction of the local integral eddy scale. As the wall is approached the integral scale decreases and so does the necessary filter width. Baggett, Jiménez & Kravchenko (1997) estimated that the number of points required for a grid satisfying those requirements scales as $N \sim Re_\tau^2$, and increases without limit with the Reynolds number. Most of those points are concentrated in the near-wall region, and the resulting resolution requirements have for some time been the main roadblock for the practical application of LES (Chapman 1979).

To decrease the number of points, one possibility would be to use fully anisotropic subgrid models correctly representing the Reynolds stresses in all the regions of the

1 School of Aeronautics, U. Politécnica de Madrid.

flow, but, as mentioned above, such models are not available at present. Another possibility is to compute the wall region by some separate technique, usually RANS, while solving the LES equations only in an interior domain away from the wall. Variants of this approach are the various proposals to use subgrid models which smoothly merge into RANS near the wall (Schumann 1975, Sullivan *et al.* 1994, Spalart *et al.* 1997).

In implementing this second class of approximations, two problems arise. The first is to provide a good model for the wall region, while the second is to transfer to the outer simulation the information obtained in this way. This implies synthesizing instantaneous boundary conditions for which only a few low-order statistics are known, but which are realistic enough to minimize the formation of spurious layers as the simulated flow adapts to the synthetic boundary. Both problems are different and essentially independent of one another. Only the second one is addressed in this paper.

To separate our investigation as completely as possible from the particular requirements of modeling wall turbulence, we restrict our computations to the lower half of a plane channel and impose our boundary conditions at the central plane, trying to mimic the information coming from the other half of the channel. Within the limits of the summer program we also restrict ourselves to direct numerical simulations, thus making our conclusions independent of the particular sub-grid model used in real LES computations.

Our problem is then to find boundary conditions that can be imposed at a fully turbulent domain boundary, using only low order statistics of the flow outside the domain, such that a direct numerical simulation approximates the statistics of the turbulent flow within. Well-known subsets of this problem are the formulations of inflow and outflow boundary conditions for turbulent flows, which have been treated often. The techniques used are different for each of them and, while outflows are usually treated by advective boundary conditions in which information is allowed to leave the domain as smoothly as possible, inflows require information coming from outside, and therefore Dirichlet conditions. A general discussion of the boundary conditions required for incompressible viscous flows is Kreiss & Lorentz (1989), and examples of particular techniques used to generate synthetic incoming turbulence at inflows are Lee, Lele & Moin (1992), Le, Moin & Kim (1997), and Na & Moin (1998).

By choosing as our boundary the center of the channel we focus on the harder problem of lateral conditions, in which the average normal velocity is either zero or small with respect to the intensity of the turbulent fluctuations, and where weak inflows and outflows coexist at locations which are not known a-priori. This is also the problem relevant to imposing conditions near walls, where information, be it provided by a separate model running in the wall layer or by the smooth merging of LES and RANS, has to flow in both directions.

Baggett (1997) studied the same problem and tried several types of boundary conditions in which the three velocity components were prescribed at an off-wall plane in a channel. The information contained in his velocities ranged from purely

random numbers to fairly complete sets of structures corresponding to real channel turbulence at the same location. His experiments were in general not successful, but the location of his boundary plane was inside the near-wall region, where turbulence dynamics is known to be most complicated, and his numerical scheme was a low-order finite-difference scheme. It was not clear whether his lack of success was due to inappropriate boundary conditions or to any of those complicating factors. In this note we largely repeat, and extend, his experiments using higher order numerics and staying away from the wall region, in order to clarify the reasons for any failure.

The note is organized as follows. The numerical technique is described first, followed in §3 by a description of the results of three different synthetic boundary conditions. That section also contains a discussion of the errors introduced in the pressure field, and of their influence on other errors in the simulation. Finally the results and their relation to the general theory of hyperbolic equations are briefly discussed and suggestions for future work are offered.

2. Simulations

2.1 Flow description

The flow simulated is the lower half of a plane turbulent channel, between the lower wall at $y = 0$ and the central plane at $y = 1$. The Reynolds number is $Re_\tau = 190$, based on the friction velocity and on the half channel width. Since the full channel is nominally symmetric, all of the energy and momentum fluxes (i.e. the mean shear stress) should be zero at the central boundary. Other properties at the boundary, when needed, are taken from the comparable simulation by Kim, Moin & Moser (1987). Wall units are defined in the usual way in terms of the friction velocity at the wall, u_τ, and used throughout the paper.

2.2 Numerical scheme

The numerical method is essentially the one used by Kim, Moin & Moser (1987). The equations are integrated in a box which is doubly periodic in the streamwise and spanwise directions, of size $L_x \times L_z = 2.7 \times 1.58$, and bounded by the center of the channel and by one wall. The spatial discretization is Fourier spectral in x and z, and fourth-order B-splines in the wall-normal direction y (Jiménez, Pinelli & Uhlmann, 1998). The nonlinear terms are dealiased in the two Fourier directions by the 2/3 rule, but there is no dealiasing in y. Time discretization is third-order Runge-Kutta for the nonlinear convective terms and implicit Euler for the dissipative ones.

The numerical resolution in x, y, and z is $48 \times 97 \times 64$ before dealiasing, and the viscosity coefficient is $\nu = 1/3250$. The grid is stretched in the wall-normal direction according to the mapping

$$y_j = \frac{1}{2} + \frac{\tanh[2\pi\kappa(2j/N - 1)]}{2\tanh(2\pi\kappa)},$$

where $j = 0 \ldots N$ and $\kappa = 0.22$. This grid is stretched both at the wall and at the central plane, which was found necessary to accommodate the spurious thin

viscous layers generated by the boundary conditions. The stretching at the central boundary could probably be relaxed if better boundary conditions are found.

The equations are written in terms of the wall-normal vorticity ω_2 and of the Laplacian of the wall-normal velocity, $\Phi = \nabla^2 v$. The evolution equations to be solved are

$$\frac{\partial \Phi}{\partial t} = h_v + \frac{1}{Re}\nabla^2 \Phi, \tag{1}$$

$$\frac{\partial \omega_2}{\partial t} = h_g + \frac{1}{Re}\nabla^2 \omega_2, \tag{2}$$

where h_v and h_g are the nonlinear terms, as defined by Kim, Moin & Moser (1987). Continuity is imposed when obtaining the velocities from the evolution variables. Pressure is not used in the evolution of the flow and is obtained only as a post-processed variable. Nonlinear terms are discretized in the y-direction by means of a collocation method, and the linear ones by Galerkin projection.

The boundary conditions in the non-periodic direction are imposed at each time substep in the elliptic dissipative substep,

$$\left(1 - \frac{\Delta t}{Re}\nabla^2\right) \omega_2^{n+1} = \omega_2^n + \Delta t\, h_g^n, \tag{3}$$

$$\left(1 - \frac{\Delta t}{Re}\nabla^2\right) \Phi^{n+1} = \Phi^n + \Delta t\, h_v^n, \tag{4}$$

$$\nabla^2 v^{n+1} = \Phi^{n+1}. \tag{5}$$

At the wall, $y = 0$, the non-slip boundary conditions can be reduced to

$$v = \frac{\partial v}{\partial y} = \omega_2 = 0. \tag{6}$$

We give the boundary conditions at the center of the channel in the form of instantaneous planes of the three velocity components, which can be reduced to v, $\partial v/\partial y$, and ω_2 using continuity. The boundary conditions for (3) are therefore Dirichlet but, for (4)-(5), they are given in terms of v and $\partial v/\partial y$ rather than Φ. They are imposed by expressing the solution as a linear combination of the following Helmholtz problems, which refer only to the boundary condition at $y = 1$.

1) A particular solution (Φ_p, v_p) of the full system (4)-(5), with homogeneous Neumann boundary conditions for Φ_p and v_p at the central plane.

2) A solution Φ_1 of (4) with a homogeneous right-hand-side and $\Phi_1 = 1$ at $y = 1$, plus the associated solution for v_1, with Φ_1 as the right-hand side of (5) and $\partial v_1/\partial y = 1$ at $y = 1$.

3) A solution v_2 of (5) with Φ_1 in the right-hand-side and $v_2 = 1$ at $y = 1$.

The solution of (4)–(5) is then

$$v = v_p + a_1 v_1 + a_2 v_2, \tag{7}$$

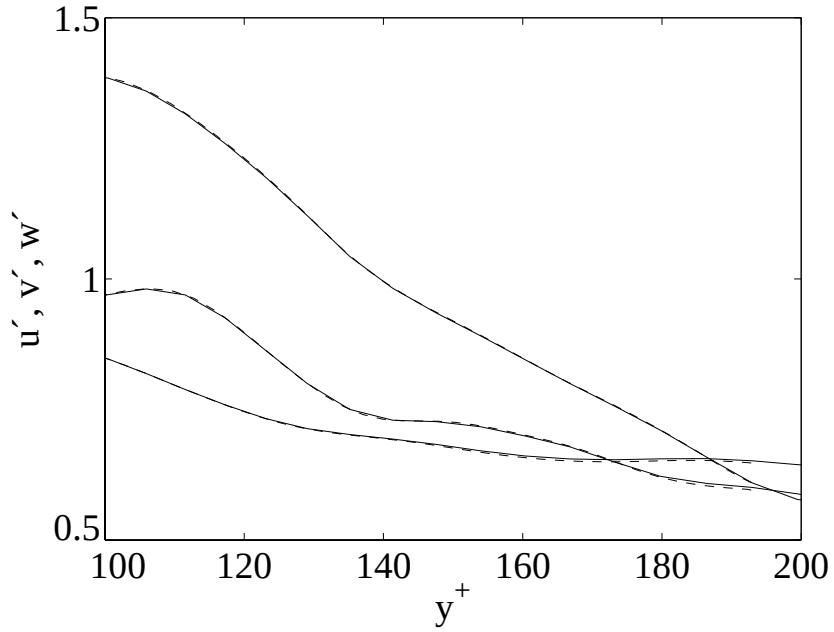

FIGURE 1. Validation of the code. ——— , full channel; - - - - , half channel. Statistics taken over 2,000 time steps ($t^+ \approx 22$).

$$\Phi = \Phi_p + (a_1 + a_2)\Phi_1, \tag{8}$$

where a_1 and a_2 are chosen to satisfy the boundary conditions.

Pressure is obtained, whenever statistics are needed, by solving (Kim, 1989)

$$\nabla^2 p = -\nabla \cdot H, \tag{9}$$

where H is the nonlinear term of the Navier-Stokes equations. The boundary conditions for (9) are obtained from the y component of the momentum equation. At $y = 0$

$$\frac{\partial p}{\partial y} = \frac{1}{Re}\frac{\partial^2 v}{\partial y^2}, \tag{10}$$

and at the center of the channel

$$\frac{\partial p}{\partial y} = -\frac{Dv}{Dt} + \frac{1}{Re}\frac{\partial^2 v}{\partial y^2}. \tag{11}$$

These manipulations are done in Fourier space, where each coefficient is a function of two wavenumbers and of the physical location, y. To simplify the notation the dependence on the wavenumbers will not be made explicit in the following. Subindices refer to position in y and superindices to the time step.

The boundary condition for the mean streamwise velocity U at the center of the channel is either Dirichlet, taken from the full-channel DNS velocity profiles, or homogeneous Neumann, which uses the condition of symmetry. In all cases the mean spanwise velocity is set to zero.

The code was validated by running first a full channel, storing a time sequence of velocities at the central plane, and then running the half-channel code, using the previously saved planes as boundary conditions at $y = 1$. Very good agreement was obtained as shown in Fig. 1, even if the grids used in both cases were very different.

3. Approximate boundary conditions

The "exact" boundary conditions at the center of the channel were then replaced by several synthetic approximations.

3.1 Case A

The first approximate boundary condition was constructed as follows. We generated a plane of the velocity component u, with the same power spectrum and intensity as those in the interior plane $y \approx 0.9$ but with random phases. The v velocity component was generated using its own power spectrum from the same plane with phases such that the shear stress $|uv^* + u^*v|$ vanished for each Fourier mode. The asterisk stands for complex conjugation. The third velocity component was generated in a similar way, satisfying $|vw^* + v^*w| = 0$. This velocity plane was computed once at the beginning of the simulation and used at each time step after applying a translation by Ut where U is the mean velocity at the center of the channel, fixed through a Dirichlet boundary condition, and set equal to the constant mean value obtained in full-channel simulations.

Unsurprisingly, the results are bad (Fig. 2a). This case is similar to the severely scrambled one of Baggett (1997). The phases of his velocity fields were also random, and a linear combination was used to obtain the correct shear stress. The main difference was that his velocities were obtained from a full-channel run and then modified, thus maintaining the correct time scales. In both his and our cases the boundary conditions are completely uncorrelated from the rest of the domain, and a strong boundary layer is created between them and the first interior plane. This is due to the lack of turbulent structure of this boundary condition as will be shown by the next experiment.

Similar results were obtained in a previous test in which the boundary condition was built in the same way, but in which the phases of the velocities were regenerated independently for each time step.

3.2 Case B

In order to provide some turbulent structure for the boundary velocities, we used a velocity plane copied directly from the previous time step in the plane $y \approx 0.9$. The velocity u was rescaled to have the same r.m.s. fluctuation u' as in the statistics of the complete channel, and the other two velocities were linearly combined to have the correct intensities v', w' and shear stresses $\overline{uv} = 0$ and $\overline{vw} = 0$,

$$u_{bc}^{n+1} = \gamma_{00} u_{y=0.9}^{n}, \tag{12}$$

$$v_{bc}^{n+1} = \gamma_{11} u_{bc}^{n+1} + \gamma_{12} v_{y=0.9}^{n}, \tag{13}$$

$$w_{bc}^{n+1} = \gamma_{21} v_{bc}^{n+1} + \gamma_{22} w_{y=0.9}^{n}. \tag{14}$$

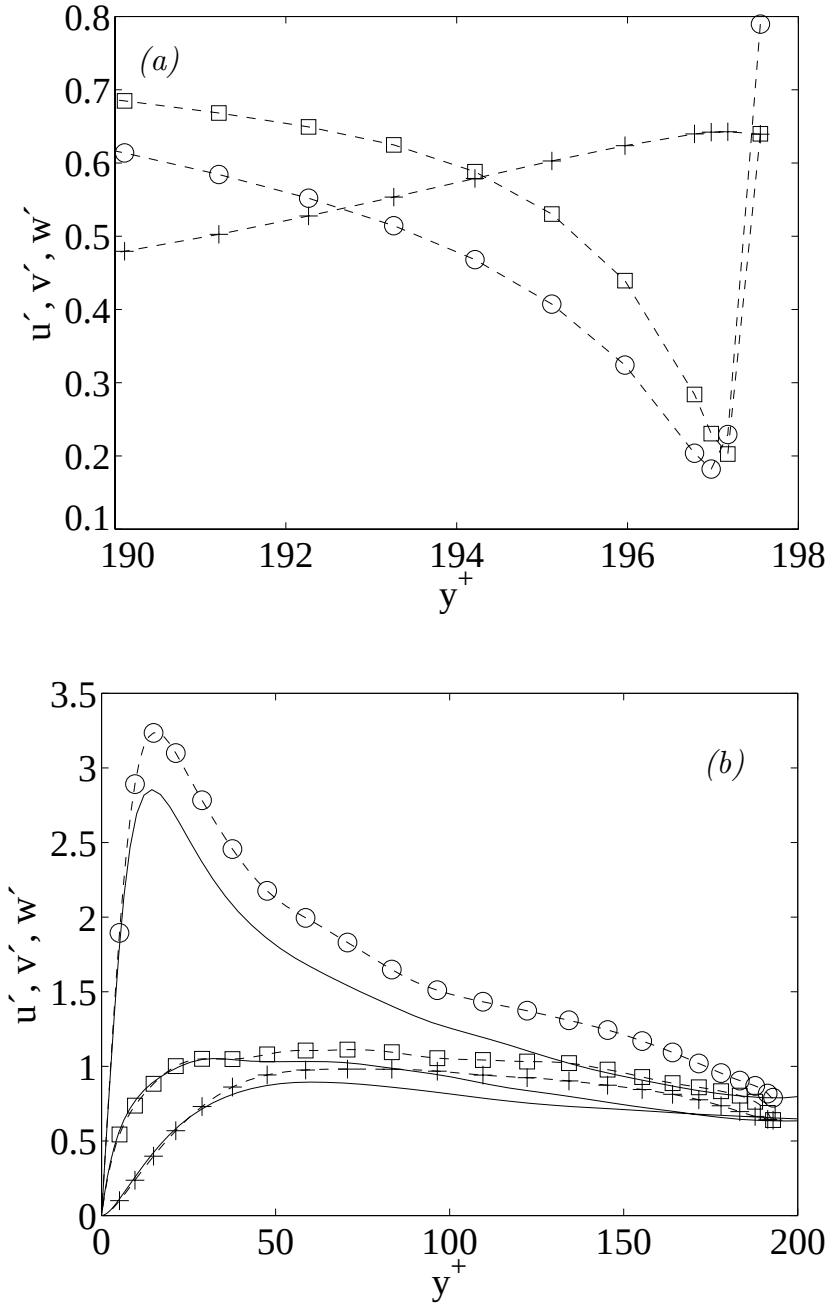

FIGURE 2. R.m.s. velocity fluctuations. ∘ , u'; + , v'; □ , w'. *(a)* Case A. $t^+ \approx 72$. *(b)* Case B. $t^+ \approx 280$. ——— , full channel.

The same constants γ_{ik} were used for all of the Fourier modes. A Dirichlet boundary condition with the correct average velocity was used for U.

In this case (Fig. 2b), the strong boundary layer disappears as the boundary condition becomes correlated with the turbulent field. Nevertheless, u', v', and w' are not well reproduced, and the mean velocity profile (Fig. 4a) changes considerably,

increasing its slope in the vicinity of the center of the channel. This experiment was not run long enough to achieve fully converged statistics since it was clear that it was evolving in the wrong direction, especially for the mean velocity profile.

3.3 Pressure fluctuations

An interesting observation was that, in the last two cases, the structure of the pressure fluctuations was very different from that in a regular turbulent channel. A large peak appears near the center line (Fig. 3a), while the fluctuations of the full channel are minimum there (Kim, 1989). This was traced to large values of $\partial v/\partial y$ near the boundary, which enter the right-hand side of (9) as random delta-function pressure sources. Essentially this is a failure of continuity, which was not taken into account in any way in the previous experiments.

While it is clear that continuity cannot be imposed on a single plane and that the flow will react to any combination of boundary conditions for u and w by adjusting $\partial v/\partial y$, this derivative can conflict with the one implied by our boundary condition for v, resulting in very large values for the effective $\partial^2 v/\partial^2 y$, and in large pressures. The problem can be visualized by thinking of the boundary condition as an artificial wall, moving randomly and forcing the flow at the boundary. Whenever the moving wall and an interior eddy collide, high pressures are generated.

To further clarify the origin of the spurious pressure fluctuations, we present in Fig. 3b the pressure for an instantaneous flow field computed in three different ways. First we use the full equation, next we zero the right-hand side of (9) in the first eight planes near the center of the channel, and finally we keep the right-hand side but zero the boundary condition (11). The main contribution to the spurious pressure is seen to be the peak of the right-hand side of (9), and once it is removed the pressure fluctuations become consistent with those of a natural channel.

Since the spurious pressure derives from the solution of a Poisson equation, it permeates the channel to a depth which is of the order of the size of the largest eddies and has a global effect on the velocity profile.

Consider the integrated equation for the kinetic energy k of the velocity fluctuations

$$\phi(y) - \phi(0) = \int_0^y (P - \varepsilon + \nu \partial^2 k/\partial y^2)\,\mathrm{d}y, \tag{15}$$

where $P = -\overline{uv}\partial U/\partial y$ is the turbulent production, ε is the dissipation, and

$$\phi(y) = \overline{v(p+k)}, \tag{16}$$

is the diffusion energy flux. If an error Δp is made in the estimation of the pressure fluctuations at the boundary, it induces an error in the energy flux which is of order $\Delta\phi = O(v\Delta p) = O(u_\tau \Delta p)$. This extra energy has to be compensated in (15) by a change in the production since the dissipation is controlled by the turbulent cascade and is difficult to change. Since the stress $\overline{uv}$ is fixed by the momentum equation, only the velocity gradient $S = \partial U/\partial y$ is available to compensate the extra energy and its error is determined by the balance

$$|\overline{uv}| \int \Delta S\,\mathrm{d}y = u_\tau^2 O(\Delta U) = O(\Delta\phi). \tag{17}$$

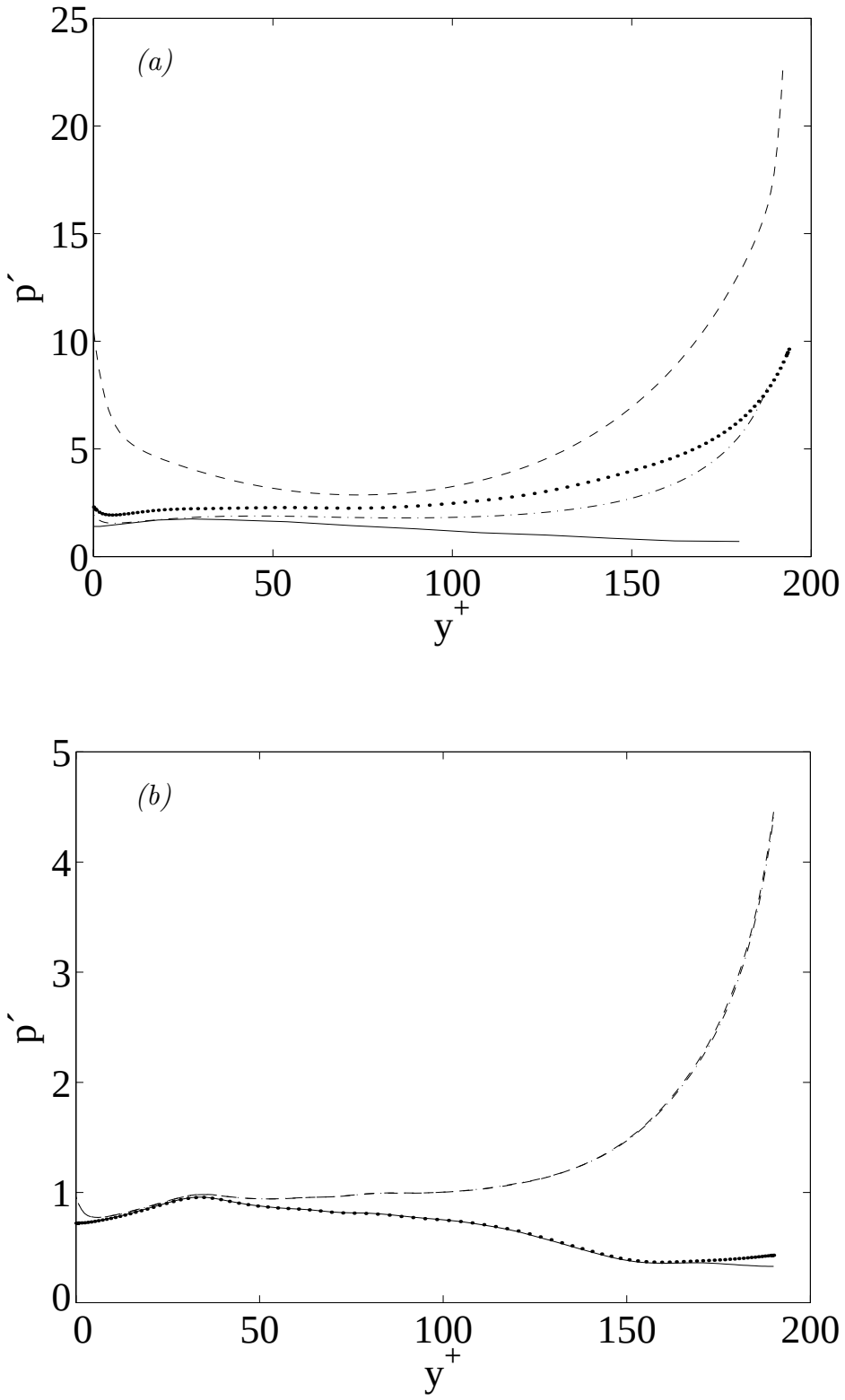

FIGURE 3. R.m.s. pressure fluctuations. *(a)* ——— , full channel; - - - - , case A; • • • , case B; —·— , case C. *(b)* Single field, case C. ——— , r.h.s. clipped and b.c. removed; • • • , r.h.s. clipped; - - - - , b.c. removed; —·— , full equation.

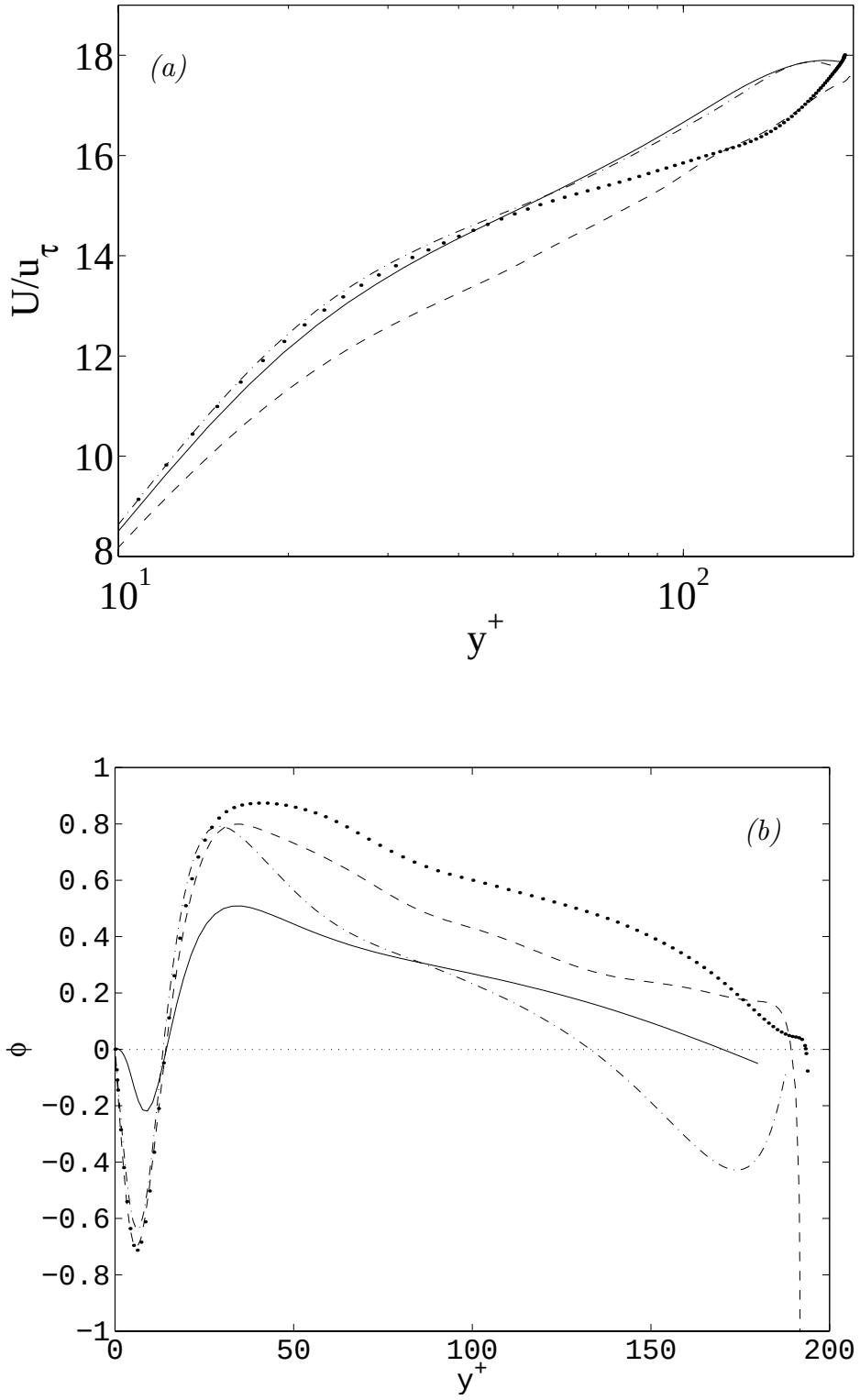

FIGURE 4. *(a)* Mean streamwise velocity. *(b)* Energy fluxes in the wall-normal direction. ——— , full channel; - - - - , case A; • • • , case B; —·— , case C.

The result is that $\Delta U^+ = O(\Delta p^+)$. Note that the effect on the mean profile can be expected to be largest near the center of the channel where the mean shear stress vanishes.

In case A where $\Delta p^+ \approx 20$, this gives errors comparable to the maximum velocity, as observed in Fig. 4a. In case B the errors in the pressure and in the mean profile, while milder, are still considerable. Note that in this figure as well as in Fig. 3, the different simulations have different values of Re_τ, both because of the errors introduced by the boundary conditions and because cases A and B were not run to full statistical convergence.

3.4 Case C

In an effort to decrease the velocity gradients at the boundary and, therefore, the magnitude of the spurious pressures and fluxes, a new condition was tried in which v at the boundary was obtained using an approximate continuity equation involving the velocities from the previous time step,

$$\frac{v_0^{n+1} - v_1^n}{\Delta y} = -\frac{\partial u_1^n}{\partial x} - \frac{\partial w_1^n}{\partial z}, \tag{18}$$

where the subindex $j = 0$ refers to the boundary plane and $j = 1$ to the first interior one. In this test u and w were copied from the plane $j = 1$ and then modified in the same way as in (12)-(14), using v in place of u and vice-versa. Previous tests had shown that the behavior of the boundary conditions was not very sensitive to the exact location of the plane from where the velocities were extracted. In this case the absolute values of the r.m.s. fluctuations were not given, and the intensities were forced to be equal in $j = 1$ and $j = 0$. This has the advantage that the correct intensities do not have to be known *a-priori* and is approximately equivalent to imposing zero derivatives for the intensities at the central plane and, therefore, to the condition of symmetry, but it should be emphasized that a Neumann condition was not imposed on individual Fourier components. A symmetry condition was also used for U, and the case was run to statistical equilibrium.

The results given in Fig. 5 are better than in the previous cases, with an agreement in the fluctuations which is particularly impressive given that their absolute values were not explicitly used at the boundary. The spurious peak pressure is also lower than before, but it is still substantial, and the Kármán constant of the mean velocity (Fig. 4a) is too low.

Figure 4b includes the energy flux for this case, which, contrary to the previous ones, is underestimated and becomes negative near the center. This means that energy is drained from the flow by the boundary condition rather than being injected as in the previous cases. It is interesting that, corresponding to this, the velocity overshoots the maximum near the central plane and then decreases slightly as the flow loses energy to the boundary. Note that the energy diffusion flux at the center of a full channel should be zero by symmetry.

4. Discussion and conclusions

We have tested several synthetic lateral boundary conditions at the central plane

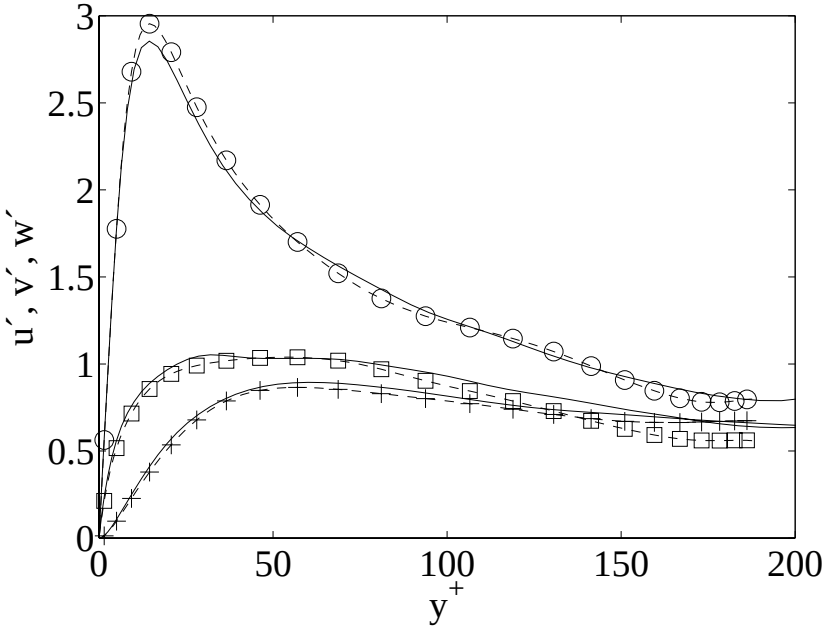

FIGURE 5. R.m.s. velocity fluctuations for case C. ∘ , u'; + , v'; □ , w'; ——— , full channel. $\Delta t^+ \approx 2134$

of a channel flow with variable success. All of them are Dirichlet conditions for the three velocity components.

Conditions with no structure, even if they have an approximately correct power spectrum but random phases, develop a sharp boundary layer and become uncorrelated with the rest of the channel. Introducing information about the turbulent structure, which was done in our case by processing data from a different plane of the same computation, considerably decreases the intensity of the spurious boundary layer and leads to reasonably good results for some of the low order statistics, namely the r.m.s. intensities of the fluctuations of u, v, and w. This is especially true when the boundary conditions are tailored to take approximately into account the continuity constraint among the three velocity components.

Nevertheless the mean velocity profiles are poorly represented. This was traced to large errors in the pressure field and in the associated energy fluxes which, even if not explicitly used in our simulation code, have fluctuations near the boundary that are an order of magnitude larger than in regular channels. This is the result of a sharp peak in the right-hand side of the Poisson equation for the pressure, and derives from the attempts of the boundary conditions to locally violate continuity. Artificially removing that local peak restores the pressure fluctuations to their proper value. The peak in the source term is confined to the first few planes near the artificial boundary ($\Delta y \approx 0.04$), and can be approximated as $B(x, z)\delta(y-1)$, where δ is Dirac's delta function. The Poisson equation for the pressure sees this forcing as a spurious boundary condition for $\partial p/\partial y$, which overwhelms the real boundary condition (11). The errors in the pressure decay exponentially away from

the boundary with a scale length which is of the order of the energy-containing scales of the intensity B. That the scale length here is of the order of the channel width shows that the errors in the boundary condition are associated with the representation of the largest eddies.

The mathematical basis for the difficulty is easy to understand. For fully turbulent boundaries away from walls, viscosity can be neglected, and it is enough to analyze the problem for the Euler equations. Note that this would also be true in LES since the eddy viscosity of the subgrid terms would in that case be at most $O(u'\Delta x)$, and the Reynolds number based on it and on the macroscopic scales would still be large. The incompressible Euler equations, except for the pressure term, are hyperbolic with characteristics which coincide with the streamlines, and this fact is widely used in the design of inflow and outflow boundary conditions (see e.g. the discussion in Kreiss & Lorentz, 1989). Incoming flow needs Dirichlet conditions because the information is brought by the characteristics entering the domain, while outgoing flow does not for similar reasons. Lateral boundaries such as the one which occupies us here coincide with characteristics implied by the mean flow, and in that approximation no boundary conditions are needed or allowed along them.

Consider for example a two-dimensional flow in which the velocity is $(U+u_1,\, v_1)$, where $|u_1|,\, |v_1| \ll U$, and where the mean velocity U is constant. The equation for the perturbation is

$$\frac{\partial u_1}{\partial t} + U\frac{\partial u_1}{\partial x} + \frac{\partial p}{\partial x} = O(u_1^2/L), \tag{19}$$

where L is a characteristic eddy size, with a similar equation for v_1. Continuity is preserved automatically to lowest order, and in that approximation the pressure satisfies Laplace's equation and can be set to zero. The resulting equation for u_1 is hyperbolic and has no explicit dependence on y. Along boundaries on which y is constant, the solution is fully determined by the inflow at $x = 0$, and no further boundary condition is needed. In fact, a Galilean transformation to a frame of reference moving with the constant velocity U reduces (19) to

$$\frac{\partial u_1}{\partial t} + \frac{\partial p}{\partial x} = O(u_1^2/L). \tag{20}$$

This is an interesting equation which shows at once that the pressure fluctuations are $O(u_1^2)$ and that the Lagrangian accelerations are of the same order. It suggests that better boundary conditions for the general case could be constructed in the form

$$\frac{\partial u}{\partial t} + u\frac{\partial u}{\partial x} + w\frac{\partial u}{\partial z} = u_\tau^2 g_u, \quad \text{at} \quad y = 1, \tag{21}$$

where u_τ acts simply as a scale for the velocity fluctuations. The information in the boundary condition, including the external statistics and length scales, is contained in g_u, which should be $O(1)$, and it is easy to see that it can be interpreted as an applied stress. Such boundary conditions are presently being tested.

The work of C. V. was supported in part by the Spanish CICYT and by INTA. J. J. was supported by AFOSR under grant F49620-97-0210. We thank J. Baggett and W. Cabot for valuable suggestions on an earlier version of this manuscript.

REFERENCES

Baggett, J. S. 1997 Some modeling requirements for wall models in large eddy simulation. *CTR Research Briefs.* Center for Turbulence Research, NASA Ames/Stanford Univ., 123-134.

Baggett, J. S., Jiménez, J. & Kravchenko, A. G. 1997 Resolution requirements in large-eddy simulations of shear flows. *CTR Research Briefs.* Center for Turbulence Research, NASA Ames/Stanford Univ., 51-66.

Chapman, D. R. 1979 Computational aerodynamics development and outlook. *AIAA J.* **17,** 1293-1313.

Jiménez, J. & Moser, R. 1998 LES: Where are we and what can we expect? *AIAA Paper 98-2891.*

Jiménez, J., Pinelli, A. & Uhlmann, M. 1998 Plane channel flow simulation over porous walls. *Tech. Note ETSIA/MF-9809,* School of Aeronautics, Madrid.

Kim, J. 1989 On the structure of pressure fluctuations in simulated turbulent channel flow. *J. Fluid Mech.* **205,** 421-451.

Kim, J., Moin, P. & Moser, R. 1987 Turbulence statistics in fully developed channel flow at low Reynolds number. *J. Fluid Mech.* **177,** 133-166.

Kreiss, H. O. & Lorentz, J. 1989 *Initial-boundary value problems and the Navier-Stokes equations.* Academic Press.

Le, H., Moin, P. & Kim, J. 1997 Direct numerical simulation of turbulent flow over a backward-facing step. *J. Fluid Mech.* **330,** 349-374.

Lee, S., Lele, S. K. & Moin, P. 1992 Simulation of spatially evolving turbulence and the applicability of Taylor's hypothesis in compressible flow. *Phys. Fluids A.* **4,** 1521-1530.

Na, Y., & Moin, P. 1998 Direct numerical simulation of a separated turbulent boundary layer. *J. Fluid Mech.* **374,** 379-405.

Schumann, U. 1975 Subgrid scale model for finite difference simulations of turbulent flows in plane channels and annuli. *J. Comput. Phys.* **18,** 376-404.

Spalart, P. R., Jou, W.-H., Strelets, M. & Allmaras, S. R. 1997 Comments on the feasibility of LES for wings, and on a hybrid RANS/LES approach, in *Advances in DNS/LES, Proc. of the 1st AFOSR International Conference on DNS/LES*, Ruston LA, August 4-8, 1997 (C. Liu, Z. Liu and L. Sakell editors), Greyden Press, 137-148.

Sullivan, P. P., McWilliams, J. C. & Moeng, C.-H. 1994 A subgrid-scale model for large-eddy simulation of planetary boundary-layer flows. *Boundary-Layer Met.* **71,** 247-276.